Supporting information

Reconfiguration of organic electrochemical transistors for high-accuracy potentiometric sensing

Luca Salvigni[1], Prem Depan Nayak[1], Anil Koklu[1], Danilo Arcangeli[1], Johana Uribe[1], Adel Hama[1], Raphaela Silva[1], Tania Cecilia Hidalgo Castillo[1], Sophie Griggs[2], Adam Marks[2], Iain McCulloch[2], Sahika Inal[*1]

[1]Organic Bioelectronics Laboratory, Biological and Environmental Science and Engineering Division, KAUST, Thuwal 23955-6900, Saudi Arabia.

[2] University of Oxford, Department of Chemistry, Oxford, OX1 3TA, United Kingdom

Corresponding Author: Sahika Inal, sahika.inal@kaust.edu.sa

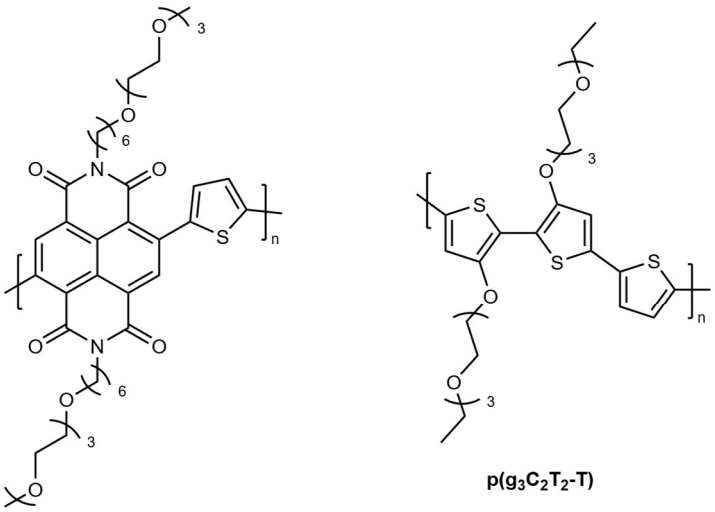

Supplementary Figure 1. n-type and p-type OMIECs. Chemical structures of the n-type OMIEC p(C_6NDI-T) and the p-type OMIEC p(g_3C_2T2-T) used as semiconductors for the OECTs and pOECTs.

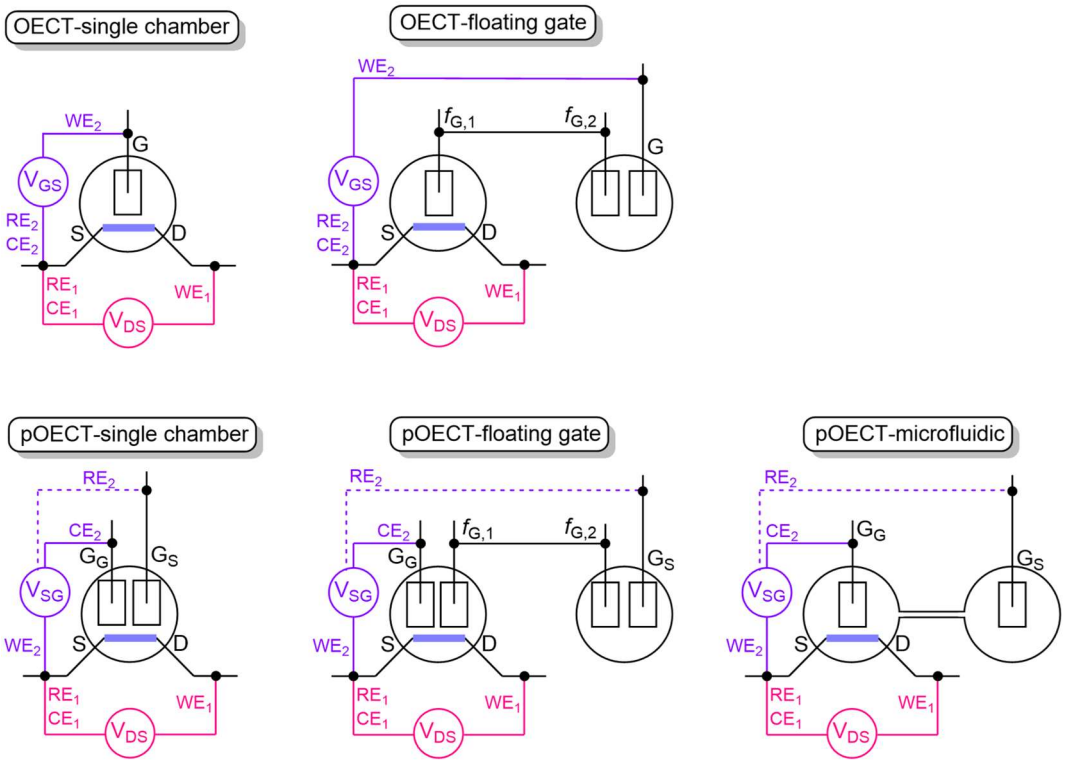

Supplementary Figure 2. Schematics of the different OECT and pOECT setups used in this work. **OECT-single chamber:** G and OMIEC are located in the same electrolyte; **pOECT-single chamber:** G_S, G_G and OMIEC are located in the same electrolyte; **OECT-floating gate:** G and OMIEC are located in two different electrolytes. The electrical and ionic communication between the sensing and amplification chambers is established through two shorted floating gates ($f_{G,1}$ and $f_{G,2}$ made of Ag/AgCl glass RE). **pOECT-floating gate:** G_S is located in a separate electrolyte while G_G and OMIEC are located in the same electrolyte. The electrical and ionic communication between the sensing and amplification chambers is established through two shorted floating gates ($f_{G,1}$ and $f_{G,2}$ made of Ag/AgCl glass RE but any other low-impedance electrode, such as Au, can be used). **pOECT-microfluidic:** G_S is located in a separate electrolyte while G_G and OMIEC are located in the same electrolyte. The electrical and ionic communication between the sensing and amplification chambers is established through a fluidic tubing that not only guarantees the ionic bridging and the closure of the electrochemical circuit but also prevents the contamination of the OMIEC chamber.

Supplementary Discussion 1: OECT/pOECT electrochemical potential measurement

The electrochemical potential of the OECT/pOECT terminals is measured during its operation by using *n* independent potentiostat channels, where each OECT/pOECT component (S, D, G, G_S, G_G) is the WE_n sharing the same RE. As an example, here in Supplementary Fig. 3, we report the electrochemical potentials of an n-type enhancement-mode pOECT device components with Ag/AgCl as G_S and a Pt coil as G_G (see pOECT transfer curve in Fig. 2a-left). The transfer curve is recorded at a constant V_{DS} = + 0.3 V, which can be seen in the graph since the D (red line) is constantly 300 mV above the S (black line). At the same time, the V_{SG} is linearly scanned from + 0.2 V to – 0.5 V, which can be seen in the graph as the distance from the S and the G_S (blue line). For a full picture, Supplementary Fig. 3 also reports the electrochemical potential of the G_G (yellow line). During the transfer curve, the G_G is slightly positively polarized when the channel is pushed to the most doping potentials.

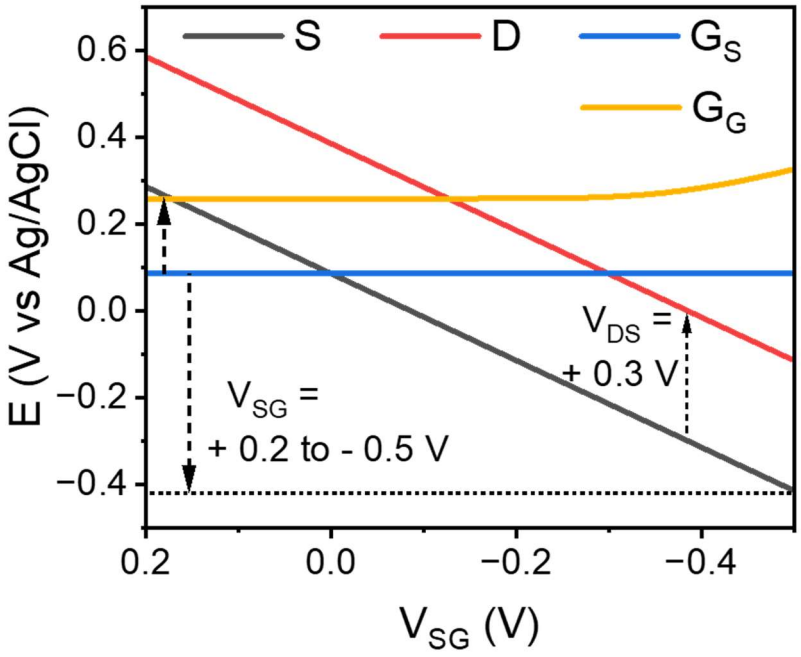

Supplementary Figure 3. OECT/pOECT electrochemical potential measurement. Electrochemical potentials of the pOECT components during the application of the voltages of a transfer curve (V_{DS} = +0.3 V and V_{SG} from +0.2 to -0.5 V).

Supplementary Discussion 2: Gate electrode polarization

Supplementary Fig. 4-left reports the transfer curves of an n-type OECT and pOECT when the G or G_S is an Au electrode of 5 mm diameter. For the OECT, it is necessary to apply a much higher gating voltage to reach the same maximum I_{DS} of the pOECT. This is due to the high G polarization caused by an increase of OMIEC capacitance/doping when pushed to negative electrochemical potentials. Supplementary Fig. 4-right shows how it is necessary to push the V_{GS} up to +1.26 V to reach the same level of OMIEC doping as with the pOECT, which then results in the same maximum I_{DS} (Supplementary Fig. 4-left). This progressive and non-linear polarization of the G leads also to a significant distortion of the transfer curve shape.

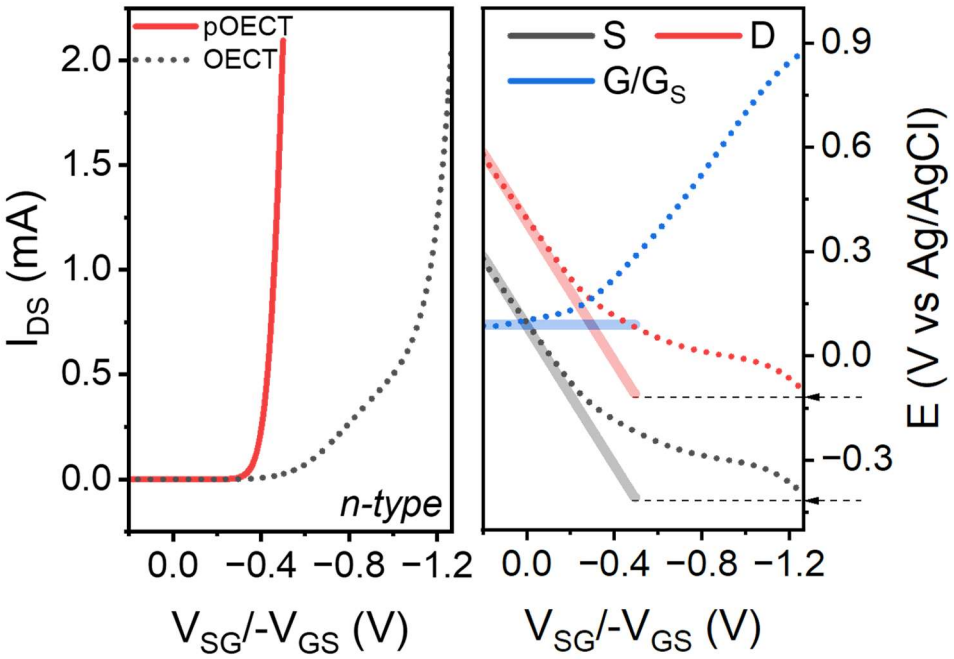

Supplementary Figure 4. Gate electrode polarization. Left: transfer curve of an n-type OECT/pOECT when a Au Φ = 5 mm is used as G/G_S and identical final I_{DS} is reached. Right: corresponding electrochemical potentials of the OECT/pOECT components during the transfer curves. The applied gate voltage is reported as V_{SG} for the pOECT and $-V_{GS}$ for the OECT. The plain lines are referred to the pOECT and the dotted lines to the OECT. The horizontal dashed arrows represent the point at which the channel of both OECT and pOECT reach the same electrochemical potential, leading to the same maximum I_{DS}.

Supplementary Discussion 3: Currents involved in the pOECT gating system and effect on the sensing electrode polarization

Supplementary Fig. 5a shows the behavior of an ideal non-polarizable electrode, which is an electrode able to keep a constant and stable potential regardless of the current flowing through it. This is a feature typical of a RE such as Ag/AgCl. Supplementary Fig. 5b shows an ideal polarizable electrode whose potential can be easily modulated even through minuscule current variations. Supplementary Fig. 5c represents an intermediate behavior, which is a characteristic of most of the electrodes, including those employed in biosensing applications. In the case of sensing based on variation of the electrochemical potential of the sensing electrode, we want to work in conditions that resemble Supplementary Fig. 5a not to lose the analytical information represented by the electrode potential. To render an electrode presented in Supplementary Fig. 5c more like the one in Supplementary Fig. 5a, we can either (i) increase the size/capacitance of the electrode or (ii) decrease the current flowing through the electrode. Increasing the size of the sensing electrode is not a practical solution for several reasons. It is not cost-efficient and does not allow miniaturization. In the case of OECTs, where the capacitance of the OMIEC is significantly higher than the materials employed in electrolyte-gated organic field effect transistors (EGOFETs), the electrode size required to achieve non-polarizability is too big for practical applications. For this reason, reducing the current passing through the sensing electrode represents a better alternative, which maintains the analytical information of the electrode potential while using an electrode of reasonable size (mm or μm range).

The main purpose of the pOECT is the removal of the OMIEC gating current from the sensing electrode (G_S), which is instead provided by an auxiliary electrode (G_G). Theoretically, through the RE cable at which the G_S is connected, no current should pass so that the potential of the RE is not disturbed and any polarization is prevented. For this reason, the impedance of the RE line is usually in the range of 1 to 100 TΩ in most of the potentiostats. However, since this impedance is high but not infinite, a small current flows through the RE. Moreover, a minimal current is required to pass through the connection, otherwise it would not be possible to measure the potential of the WE with respect to the RE, and apply the required V_{SG}, because the RE would result as completely disconnected from the circuit. As a demonstration of this feature of the potentiostat circuit, we report the schematic of a classical 3-electrode setup operated with a potentiostat in Supplementary

Fig. 5d**.** The presence of the electrical currents involved in the circuit is highlighted with grey arrows. One of these currents is the one flowing between the WE and the CE (I_{WE}), which is normally reported in a cyclic voltammetry (CV) or linear scan voltammetry (LSV) plot. The other one is the current flowing through the RE (I_{RE}). Supplementary Fig. 5e reports these two characteristic currents in the case of the oxidation scan of an Au Φ = 5 mm WE in a 1x PBS solution of 10 mM ferrocyanide. Due to the high impedance of the circuitry associated with the RE, the I_{RE} is 9 orders of magnitude lower than I_{WE}. However, the shape of the I_{RE} follows the same trend as the I_{WE}, demonstrating that any increase in the I_{WE} will also be reflected in the I_{RE} but on a much lower order of magnitude. The magnitude of the I_{RE} is proportional to the total current flowing through the circuit, which can be estimated from the I_{WE}. This total current depends on the properties of the electrochemical cell, such as WE size and concentration of redox active components. To demonstrate the proportionality of the I_{RE} with the I_{WE}, we report an analogous measurement performed with WEs of different sizes in Supplementary Fig. 5f. A WE of larger size (larger area) provides a higher I_{WE} (Supplementary Fig. 5f-left, bottom) whose intensity follows the proportionality with the electrode size (Supplementary Fig. 5f-left, top). The same current trend is also reflected on the I_{RE} (Supplementary Fig. 5f-right, bottom) with an analogous proportionality (Supplementary Fig. 5f-right, top) but with an intensity 9 orders of magnitude lower with respect to the I_{WE}; the relationship for this specific case between the I_{RE} and I_{WE} is about 2 pA(I_{RE})/1 mA(I_{WE}), $R^2 = 0.998$. This experiment demonstrates that despite the negligible I_{RE}, if the size of the WE increases or the electrochemical cell is miniaturized, the non-polarizability of the RE is sacrificed. As such, the RE could become polarized, reducing the reliability of the analytical method, a condition, however, which rarely occurs.

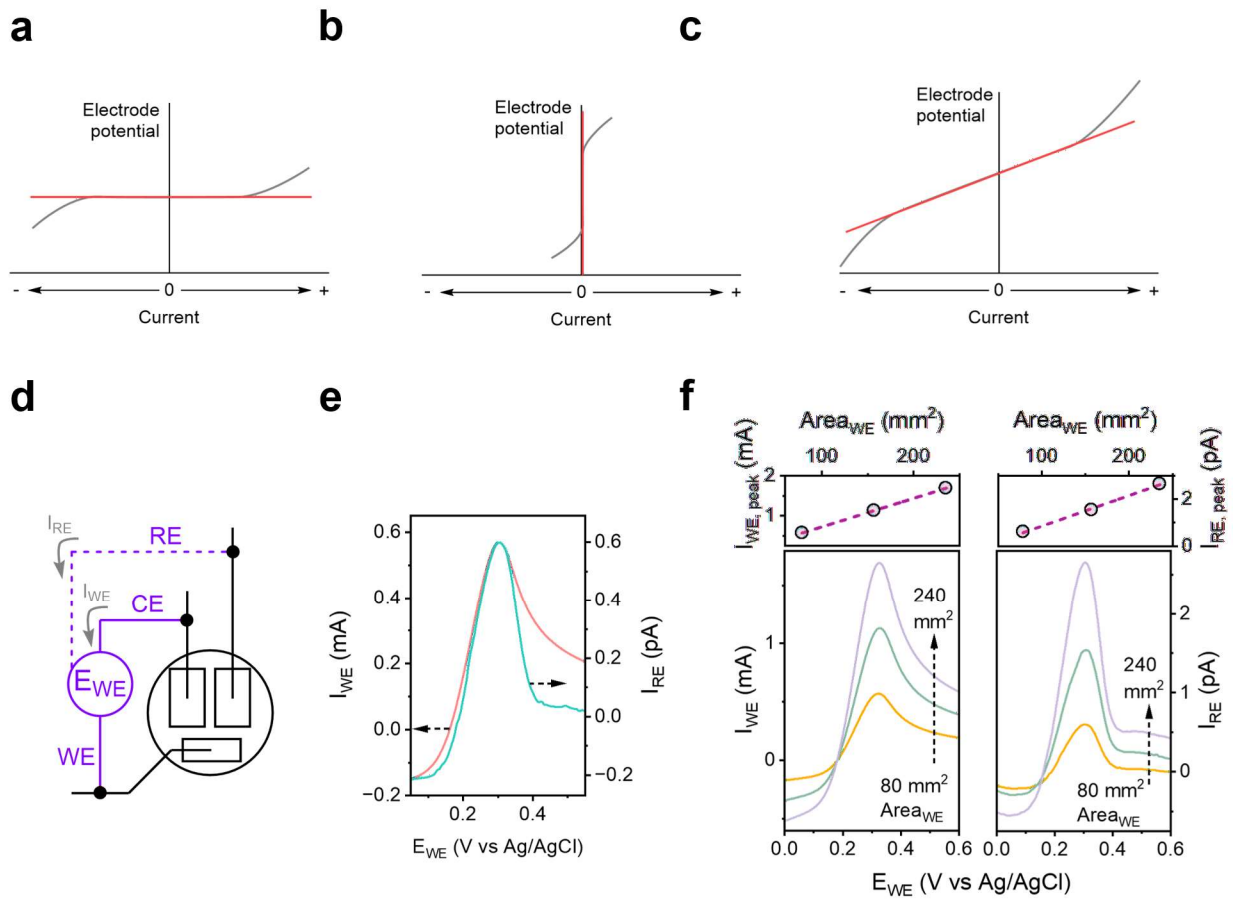

Supplementary Figure 5. **Reference electrode current in a traditional 3-electrode setup.** Schematic behavior of the electrode potential as a function of the current for **a)** an ideal non-polarizable electrode, **b)** an ideal polarizable electrode, **c)** an electrode with an intermediate behavior. The red line represents the theoretical ideal behavior, and the grey line represents the real behavior. **d)** Schematics of a 3-electrode cell with the currents involved in the circuit: the current flowing through the WE (I_{WE}) and the current flowing through the RE (I_{RE}). The dashed line represents the high impedance connection of the potentiostat, and the large black circle represents the electrolyte. **e)** LSV of a Φ = 5 mm Au WE in a solution of 1x PBS and 10 mM ferrocyanide, where in pink line represents the I_{WE} and the green one is the I_{RE}. **f)** LSV of Au WE of different areas in a solution of 1x PBS and 10 mM ferrocyanide. I_{WE} (left) and I_{RE} (right) as a function of the applied potential (bottom) and the correlation between the peak current and the WE area (top).

For the pOECT, we can consider the current flowing through the G_G (I_{G_G}), which is the current that effectively dopes and dedopes the OMIEC, as the I_{WE}, and the current flowing through the G_S (I_{G_S}) as the I_{RE}, due to the analogous cable connections to the 3-electrode setup, as shown in Supplementary Fig. 6a. It is important not to confuse the I_{GS} (also called I_G) of a classical OECT

setup and the I_{G_S} of the pOECT setup, where ideally $I_G = I_{G_S} + I_{G_G}$ since RE and CE connections are shorted on the same electrode. To increase the current flowing through the gating system, analogous to what is shown in Supplementary Fig. 5f, we can increase the thickness of the OMIEC film in the channel. In Supplementary Fig. 6b, we report transfer curves for two pOECTs with either a thick or thin layer of OMIEC channel. The thick pOECT shows a slightly lower I_{DS} (for a constant scan rate) due to its slower behavior. If the amount of OMIEC that has to be doped at the applied voltage (V_{SG}) increases (Thin → Thick), also the doping current (I_{G_G}) has to increase, as shown in Supplementary Fig. 6c-left. Similar to what we saw in the LSV curve (Supplementary Fig. 5e), the I_{G_S} is higher, but remaining always 6 or 7 orders of magnitude lower than the I_{G_G} (Supplementary Fig. 6c-right). This experiment demonstrates that, even if the pOECT guarantees no-polarization for the sensing electrode, this is not true in absolute terms. If the size of the G_S is extremely small (nm or tens of µm), the G_S material is poorly conductive, or the amount of OMIEC in the channel is high, the G_S could be polarized even with few tens of pA of current. However, for the most common biosensing applications, where the channels have µm size, and the sensing electrode sizes are in the mm range and are made of noble metals, metal oxides, OMIECs, or carbon-based materials, the pOECT setup allows the prevention of any polarization of the sensing electrode. Moreover, if G_S is required to be in µm dimensions, such as for brain activity monitoring[1], the electrodes can be functionalized with an OMIEC layer like PEDOT:PSS[2] to increase their capacitance and reduce the polarizability.

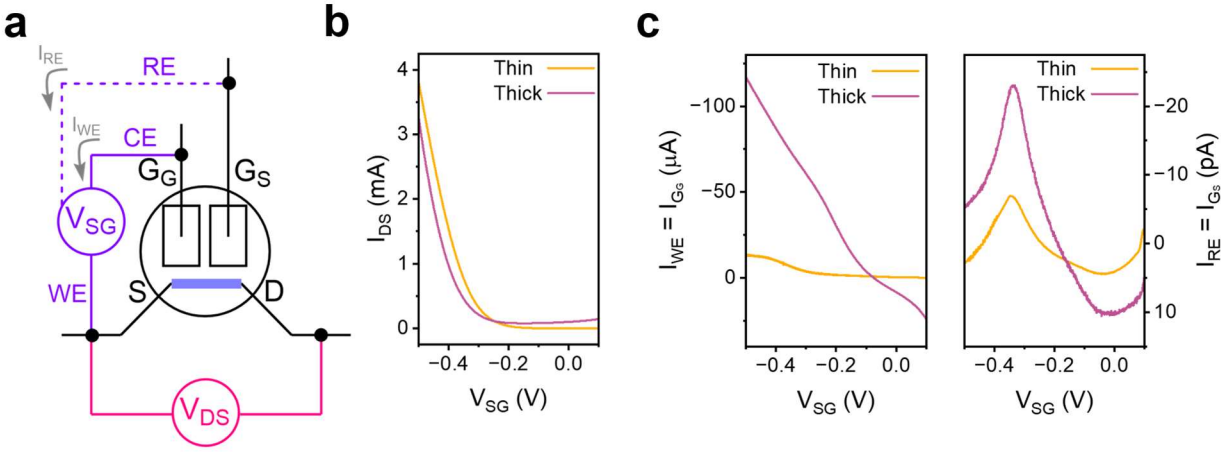

Supplementary Figure 6. Reference electrode current in a pOECT. a) Schematics of a pOECT with only the electrodes involved in the gating system labeled. The grey arrows highlight the currents involved in the gating circuit: the current flowing through the G_G ($I_{WE} = I_{G_G}$) and the

current flowing through the G_S ($I_{RE} = I_{G_S}$). The dashed line represents the high impedance connection of the potentiostat, and the large black circle represents the electrolyte. **b)** Transfer curves of an n-type pOECT with either a thin or thick layer of OMEIC deposited on the channel. **c)** I_{WE} (left) and I_{RE} (right) recorded during the operation of the two transistors with a thin or thick layer of n-type OMIEC.

As a demonstration of an exceptional case where the G_S can be polarized by the I_{RE}/I_{G_S}, we report in Supplementary Fig. 7a a pOECT in which the G_S is a classical pH-meter glass electrode. The experiment reported here is the same as the one presented in Fig. 4g at pH = 10. One of the cases that could lead to a G_S polarization even with the small pA current passing through the RE (I_{RE}) is the poor conductivity/high resistance of the G_S. In the case of a classical pH-meter, the pH sensitive component is a glass membrane whose resistance is typically 50-500 MΩ. This would normally lead to an extremely high gating voltage drop across the glass membrane if used as a direct G in a classical OECT setup ($V_{drop} = R_{membrane} \times I_G = 50 \cdot 10^6 \times 100 \cdot 10^{-6} = 5$ kV). However, since in a pOECT the current flowing through the G_S is several orders of magnitude lower, the voltage drop reaches an acceptable value. Considering the glass membrane resistance as 50 MΩ and an I_{RE} of 20 pA, the V_{drop} is equal to 1 mV ($V_{drop} = R_{membrane} \times I_G = 50 \cdot 10^6 \times 20 \cdot 10^{-1} = 1$ mV). This value is in agreement with what is measured by monitoring the electrochemical potential of the pOECT components **(**Supplementary Fig. 7b-left) where the potential of the G_S is oscillated/polarized around an average value with an amplitude of ± 1 mV (Supplementary Fig. 7b-left, top). Despite the small voltage drop, this polarization is not harmful. The V_{drop} measured for the G_S is one order of magnitude lower than the usually applied amplitude modulation in electrochemical impedance spectroscopy (EIS), which is considered a non-destructive technique (if the modulation is applied vs. OCP hence, analogous conditions as in Supplementary Fig. 7b for the G_S). We can further verify that this small polarization has no effect on the electrochemical state of our electrode if we compare the electrochemical potential of the G_S before the device operation (-180.2 ± 3 mV vs. Ag/AgCl) and during the device operation (-180.5 ± 6 mV vs. Ag/AgCl). Moreover, the drift of the G_S potential during the pOECT operation is about -2 μV/s, which is widely inside the usual drift range of a resting RE[3].

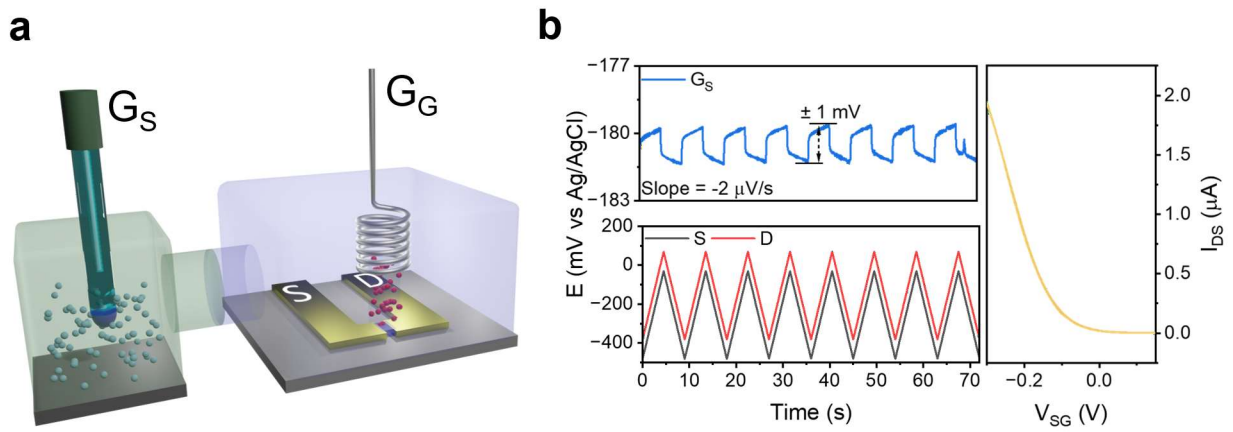

Supplementary Figure 7. Effect of the pOECT I_{RE} on a high-impedance sensing electrode. a) Visual representation of a pOECT in which the G_S is a high impedance electrode (i.e., a glass membrane pH-meter). **b)** Electrochemical potential of the G_S (top) and S and D (bottom) during n-type pOECT operation through a cyclic repetition of transfer curves. Right: The transfer curves.

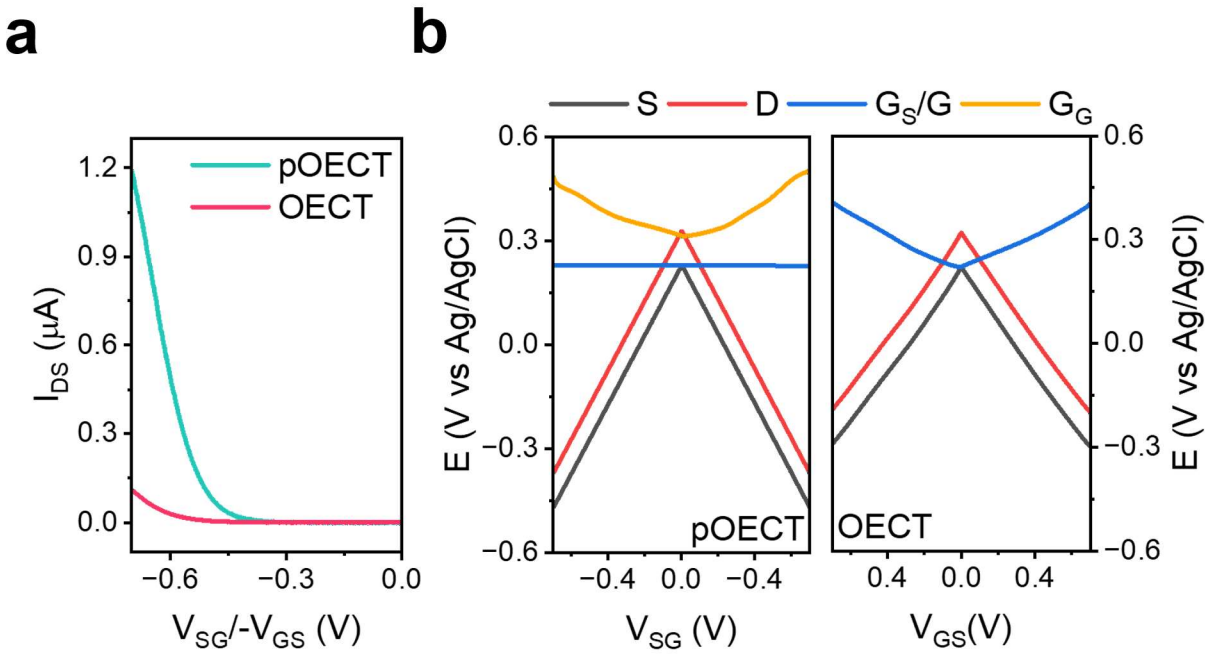

Supplementary Figure 8. Performance comparison of a miniaturized OECT and pOECT. a) Transfer curves of microfabricated pOECT and OECT with a 100x10 µm channel and a 500x500 µm G, G_S and G_G. The plot shows the different I_{DS} modulation capabilities of the two configurations. **b)** Electrochemical potentials of the microfabricated pOECT and OECT components during the transfer curve.

In Supplementary Fig. 8, we compare the electrochemical performance of microfabricated OECT and pOECT of similar size. The devices have identical channel (100x10 µm) and sensing interface (500x500 µm, G and G_S) dimensions. The only difference for the pOECT is the additional electrode (G_G) of the same size as the sensing interface. The overall substrate size and active area are exactly the same in both devices. Similar to the devices with vertical gating electrodes, the pOECT allows a much larger I_{DS} modulation (Supplementary Fig. 8a). In the OECT, the G polarizes during the V_{GS} application, even if the electrode has a surface area 250 times higher than the channel (Supplementary Fig. 8b-right). This polarization is instead efficiently prevented by the pOECT (Supplementary Fig. 8b-left), where G_S remains unperturbed at its stable equilibrium electrochemical potential, and the auxiliary electrode (G_G) plays the role of doping the OMIEC, being consequently polarized. In addition to its stable and high performance, the pOECT is as miniaturized as the conventional OECT, as exemplified here.

Supplementary Discussion 4: pOECT miniaturization capabilities and comparison with OECT dimensions

As demonstrated in Supplementary Fig. 8 and Fig. 4a-b, an OECT with a comparable electrode size as a pOECT (OMIEC and sensing interface area) has an output signal with severe interference from gate polarization. The polarization renders the OECT in this geometry either a poor sensor (due to low modulation) or a sensor with inaccurate output (as the polarization affects the channel current). To achieve the same accuracy as the pOECT, we need to operate the OECT with a very large G. However, the necessary size to make this electrode non-polarizable exceeds the acceptable dimensions for a portable device. A partial demonstration of this is reported in Fig. 2c-right and Supplementary Fig. 3. Despite the large capacitance of the G_G granted by a 23 cm long Pt wire, the electrode is still polarized (+65 mV) by the leakage current necessary to dope the channel. Hence, if this electrode is used as G in an OECT, it will still be polarized.

With organic semiconductors employed for EGOFETs, a millimeter gate size is sufficient to prevent any polarization and provide reliable performance, as demonstrated in previous works[4–6]. With OMIECs, the doping mechanism involves the entire bulk of the transistor channel, requiring a larger number of ionic charges and, in turn, a larger I_{GS}. The result is that for OMIEC-based transistors, even the large area gates[7] of EGOFETs biosensors are not large enough to prevent the polarization of the G.

For example, Supplementary Fig. 9a shows the transfer curves of a pOECT in which the G_S is a very small Au electrode (170 μm in diameter) and an OECT in which the G is a Au electrode, the size of which is progressively increased from a diameter of 170 μm to 1 cm. The pOECT shows a full I_{DS} modulation up to 1.5 mA, with a minimal G_S polarization of 1 mV as reported in Supplementary Fig. 9b-i. Note that, as already demonstrated in Fig. 2c, the size optimization of the G_G is not crucial for determining the pOECT performance. Hence, in this experiment, we used an Au electrode of 1.6 mm diameter as G_G. When the same small G_S is used as G in an OECT (Supplementary Fig. 9a, right), the I_{DS} modulation is absent because the applied V_{GS} drops almost entirely on the G itself (684 mV polarization), as demonstrated in Supplementary Fig. 9b-ii. If we want to bring the I_{DS} modulation of the OECT to the same level as the pOECT, we need to increase the size of the G. By progressively increasing the G diameter from 170 μm up to 1 cm, we observe a gradual increase in I_{DS} modulation, Supplementary Fig. 9a-right. The increase in G size reduces

the G polarization gradually, as shown in Supplementary Fig. 9b-ii-iv. However, even with a G diameter of 1 cm, which corresponds to an area 4200 times larger than the G_S of the pOECT, the G is still polarized (97 mV), Supplementary Fig. 9b-iv, leading to a lower I_{DS} modulation compared to that of a pOECT operated with a much smaller sensing interface.

If we correlate the measured G polarization with the G diameter or area, we obtain the trend reported in Fig. 4c. We observe an exponential decrease of the G polarization with size, but the G polarization is comparable to the G_S polarization only when the G reaches a diameter of 4 cm. This demonstrates that an OECT with an equivalent accuracy as the pOECT (minimal sensing interface polarization) requires the G to be 55-thousand times larger. Even when we consider the total gating area of the pOECT (i.e., the size of the G_G plus that of the G_S), the pOECT gating system area is 625 times smaller than that of the OECT ($A_G/(A_{GS}+A_{GG})$).

We can conclude that an OECT with comparable performance as a pOECT requires a gate electrode of unpractical size. Hence, the pOECT, despite the integration of a second electrode, remains smaller than an OECT designed for potentiometric sensing applications.

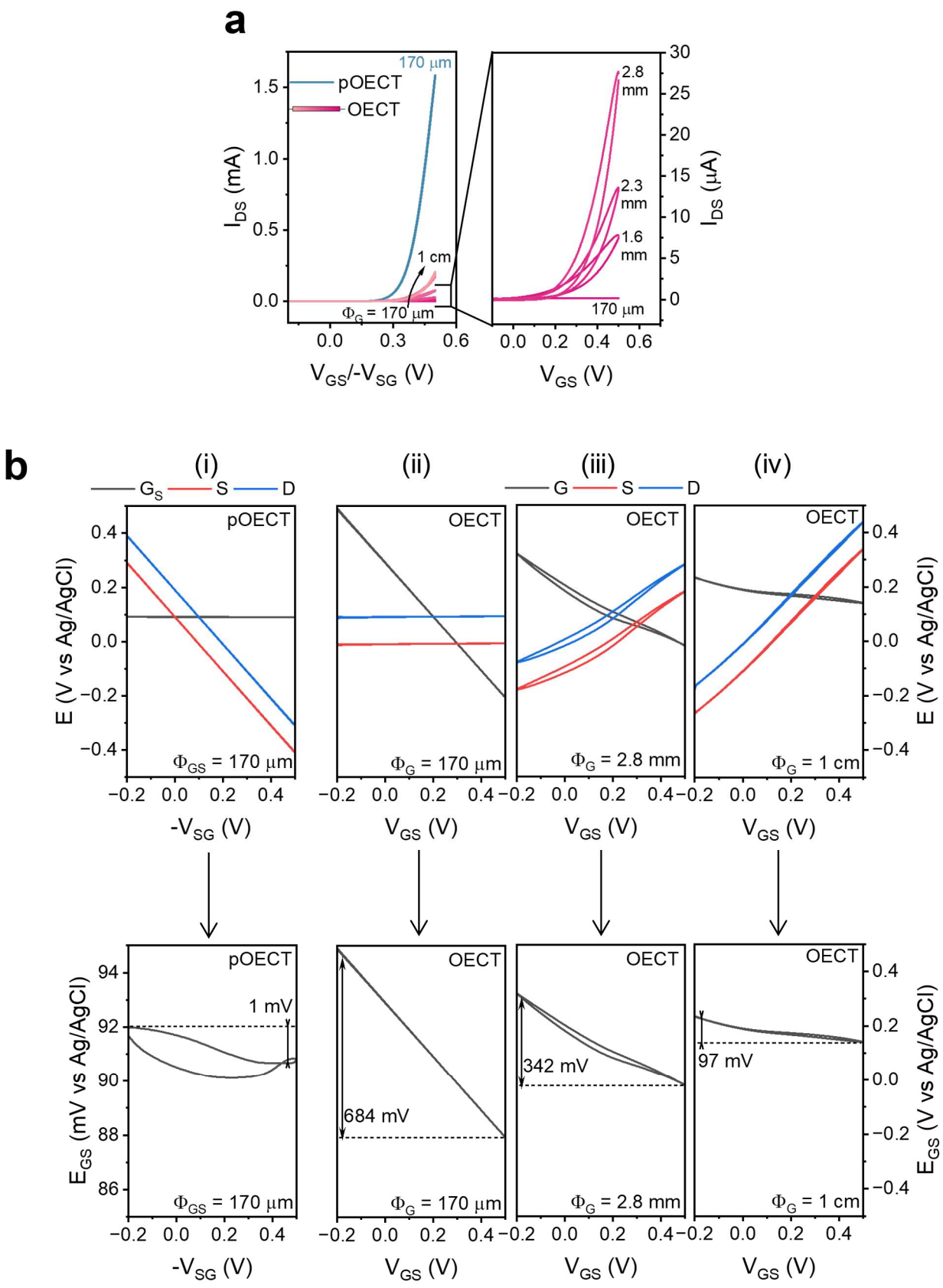
a
170 µm
pOECT
OECT
1 cm
Φ_G = 170 µm
2.8 mm
2.3 mm
1.6 mm
170 µm
I_{DS} (mA)
I_{DS} (µA)
V_{GS}/-V_{SG} (V)
V_{GS} (V)
b
(i)
(ii)
(iii)
(iv)
G_S S D
G S D
pOECT
OECT
Φ_{GS} = 170 µm
Φ_G = 170 µm
Φ_G = 2.8 mm
Φ_G = 1 cm
E (V vs Ag/AgCl)
-V_{SG} (V)
V_{GS} (V)
1 mV
684 mV
342 mV
97 mV
E_{GS} (mV vs Ag/AgCl)
E_{GS} (V vs Ag/AgCl)

Supplementary Figure 9. Sensing electrode polarization vs size in OECT and pOECT. a) Left: Transfer curves of a pOECT (blue; operated with G_S of Au- 170 µm of diameter and G_G of Au- 1.6 mm of diameter) and an OECT (pink; operated with G electrodes with a diameter ranging from 170 µm to 1 cm. Right: zoomed-in OECT transfer curves. **b)** Electrochemical potential changes of the OECT/pOECT components during the transfer curves, for a specific G/G_S diameter (Φ). The bottom panel shows the electrochemical potentials exclusively for the G/G_S, reporting the total electrode polarization.

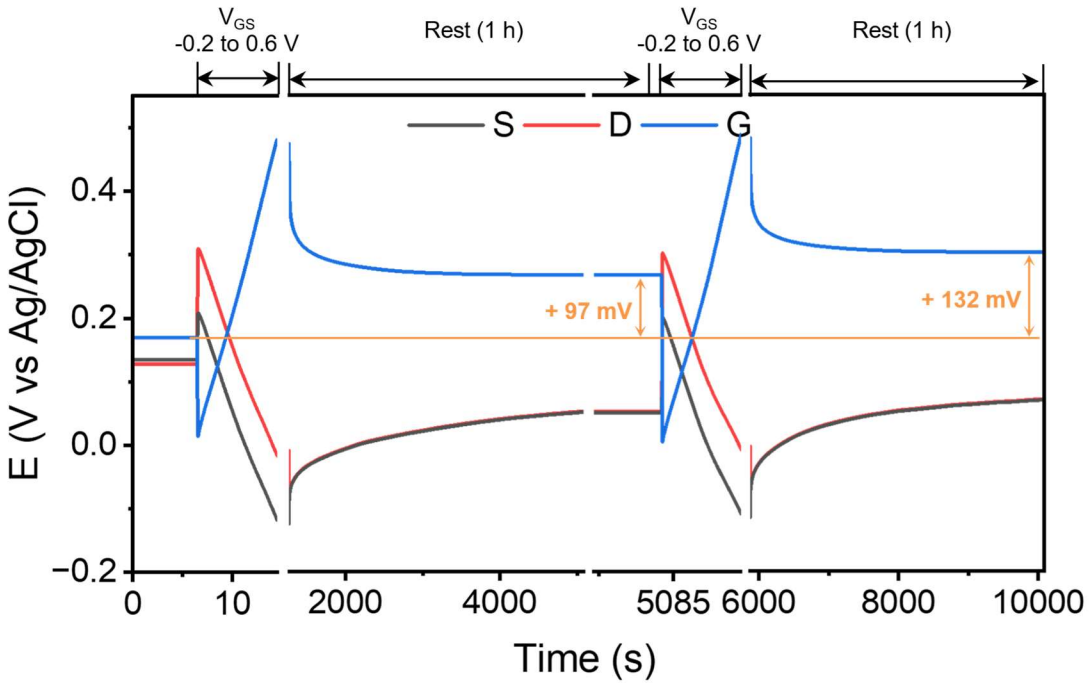

Supplementary Figure 10. Permanent alteration of the sensing electrode potential upon OECT operation. Electrochemical potential vs time of the n-type OECT components during two consecutive sets of 50 transfer curves each, separated by a resting period. No voltage is applied until the 5th second, followed by the recording of the first transfer curve of the first set (V_{GS} -0.2 to 0.6 V); the subsequent 49 cycles are not displayed. At the end of the first set, there is a 1h resting period during which no voltage is applied. This period shows a new equilibrium potential of the G due to the I_{GS} which leads to a permanent increase of the electrode surface potential of 97 mV. This increase represents the permanent change of the electrode properties, i.e., a new potential and loss of any analytical information. This also causes a different output current in the second set of transfer curves (after 5000 s) and a further change of the equilibrium surface potential of the sensing electrode (+132 mV).

Supplementary Discussion 5: Nernstian and Super-Nernstian response of pOECT and OECT

An OECT/pOECT cannot improve the response of the sensing interface from Nernstian or sub-Nernstian to super-Nernstian but just convert the voltage response to an amplified current response or another form of OECT-related voltage. The Nernstian sensitivity is defined, for example, as ±59 mV/dec for an ISE for monovalent ions or a pH sensor. What is frequently mistakenly considered correct is that any output voltage of an OECT (or more complex configurations), such as V_{DS}, g_m peak position or more, can be attributed to the Nernstian voltage. The Nernst equation describes the electrochemical potential of the sensing interface in an OCP condition, which is in the absence of current and with the sensing interface at its thermodynamic equilibrium. Most of the works claiming OECTs with Nernstian or Super-Nernstian sensitivities do not report any electrochemical potential measurement of the sensing interface during the OECT operation that can allow to verify if this claim is correct. For this reason, here we discuss only the results obtained by Gualandi et al., who performed a systematic analysis and reported all the necessary data for different examples of OECTs driven by potentiometric signals. In their first OECT-based pH sensor[8], they employ poly(3,4-ethylenedioxythiophene:bromothymol blue (PEDOT:BTB) as G and monitor as output signal the position of the OECT g_m peak as a function of pH. The resulting shift of the g_m peak is -93 mV/pH, which is claimed to be a Super-Nernstian response. This claim is theoretically incorrect since the reported voltage is not an electrochemical potential of PEDOT:BTB during its operation in the OECT. In subsequent work,[9] the authors show how PEDOT:BTB in a 2-electrode OCP measurement exhibits a sensitivity of -43 mV/pH, below the super-Nernstian response. In this work, they also monitor the electrochemical potential of this material when used in the OECT channel during the pH sensing, revealing a sub-Nernstian sensitivity of 5 mV/pH, which, however, still allows to have an appreciable calibration curve thanks to the amplification provided by the OECT. The loss of 38 mV/pH when the pH sensitive material is under the application of a voltage/current that disturbs the thermodynamic equilibrium established by the Nernst equation is analogous to what we show in Fig. 4b. This conclusion does not mean that a Super-Nernstian OECT is not possible to achieve. Gualandi et al. developed another OECT-based pH sensor using PEDOT:PSS/iridium oxide (IrOx) nanoparticles[10]. This material already showed a Super-Nernstian response of -81 mV/pH when employed in a classical 2-electrodes setup for OCP measurement. The electrochemical potential of the material, when used in an OECT, showed a

sensitivity of -64 mV/pH. Only in this case the OECT also have a Super-Nernstian response because the intrinsic material behavior is partially retained in the OECT configuration. The partial loss of sensitivity of 17 mV/pH is probably again due to the voltage applied to the OECT components that do not allow the material to settle at the thermodynamic equilibrium.

Supplementary Discussion 6: details on the thermodynamic advantages of pOECT over OECT

To the best of our knowledge, the first example of OECT sensor designed to respond to variations of the electrochemical potential of the G in a Nernstian manner (hence thermodynamic response), is reported by Gualandi et al.[11] Their OECTs represent the closest analogous to classical potentiometric sensing in a 2-electrode setup, and for this reason, their work will be taken as a reference point. The authors showed how an Ag/AgCl gate electrode can modulate the I_{DS} of an OECT depending on the concentration of Cl^- in the electrolyte in contact with the AgCl wire, following the Nernst equation. The same group developed other OECT-based potentiometric sensors, for the detection of other ions[12] and pH[8–10], with different OECT architectures, such as dual terminal and Wrighton-configuration. In these works, the authors list or indirectly show a series of limitations that our pOECT can overcome. For example, the use of redox active species as a sensing element[11] narrows down the range of possible voltages that can be applied to the OECT due to the parasitic faradaic reactions of the sensing material, leading to its oxidation or reduction. This problem is avoided in the pOECT because the sensing interface is maintained in an OCP configuration.

The authors also introduced the concept of electrochemical gating[13], where the conductivity of a channel, electrically shorted with the gate[12], or inside which the gating material is dispersed[11], can be modulated through spontaneous electrochemical reactions without a gate voltage. This configuration simplifies the OECT design because it removes the application of the gate voltage[12] or completely removes the gate electrode[11] but, at the same time, is equivalent to operating the OECT at V_{GS} = 0 V. This operating condition may not represent the voltage at which the OECT guarantees the highest sensor response, as shown for example in Fig. 3f. Moreover, while the sensitivity of an ISE depends only on the charge of the detected ion (according to the Nernst equation), in an electrochemically gated OECT, the behavior is different. Since the electrochemical potential of the S is equal to the electrochemical potential of the G ($E_S = E_G$) at any time, the channel is biased around different electrochemical potentials (doping states), depending on the intercept value of the Nernst equation that describes the specific potentiometric interface, which then corresponds to different sensitivity regimes for the OECT. This leads to anomalous behavior compared to the Nernstian one, where despite the same charge of the ion, different ionic species (such as Cl^-, Br^-, I^-) show different sensitivity due to different k values. With the pOECT

configuration, it is still possible to apply any desired V_{GS}, not only 0 V. The voltage is provided by an independent CE (G_G) and the channel can always be at the voltages where the pOECT shows the highest response, regardless of the k that describes the thermodynamic equilibrium of the G_S. This allows us to operate the device at an electrochemical potential close to the onset potential of the OMIEC[12] at the maximum transconductance efficiency[14]. The authors also point out that the electrochemical gating can work only if the gate or the gating material has a much higher capacitance than the channel, to bring the Fermi level of the channel to the same level of the G, without affecting the Fermi level of the G itself. This requirement can be reached only with a large size or a non-polarizable G. Also, in this case, with the pOECT, the modulation of the Fermi level of the channel is provided by an independent electrode (G_G), whose characteristics do not affect the pOECT performance, removing the requirement of non-polarizability of the G. They also show that a voltage applied to the potentiometric electrode hampers the spontaneous redox processes required to reach the thermodynamic equilibrium and stable potential[9].

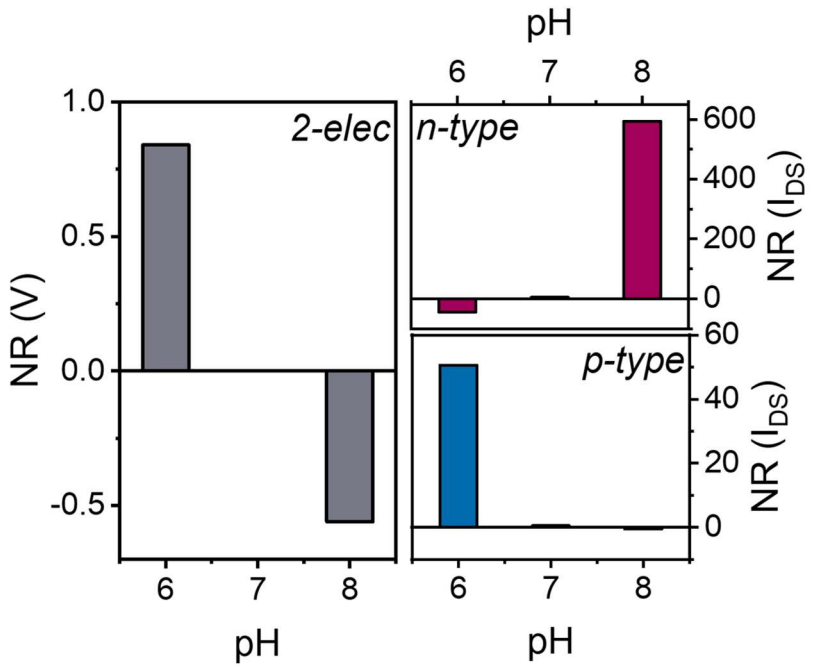

Supplementary Figure 11. Complementary pOECT performance improvement through channel size optimization. Normalized responses of the n-type and p-type pOECT with interdigitated channels and the classical 2-electrode setup when the sensing electrode is exposed to electrolytes with different pH values.

Since intrinsically-undoped OMIECs have naturally low OFF currents, increasing the size of the transistor channel increases the maximum ON current, leading to a higher NR for the same electrochemical potential shift of the G_S. In Supplementary Fig. 11, we report the NR of a complementary pOECT where the channel size increased from W·L=100·10 µm to 980 mm · 5µm, leading to channels capable of reaching mA current ranges. In this case, the pH shifts tested are only one unit (smaller than the ones reported in Fig. 6b), leading to a p-type NR of 51 and an n-type NR of 594. With a larger channel, the performance of the n-type device is significantly higher since it corresponds to one order of magnitude more for an input signal three times smaller (3 orders of magnitude smaller if we consider the ion concentration and not the logarithm) than the experiment reported in Fig. 6b. The increase in performance of the p-type device is still remarkable because it retains a similar NR value but for a pH shift three times smaller. However, the n-type device performed better because, regardless of the channel size, the material can keep its OFF current in the range of units of nA or even hundreds of pA. Instead, the p-type OMIEC has a higher OFF current when the channel is larger (tens of nA vs. tens of µA), due to the spontaneous oxygen doping[15].

Supplementary Discussion 7: Identification of the optimal Gs electrode for cell monitoring with pOECT

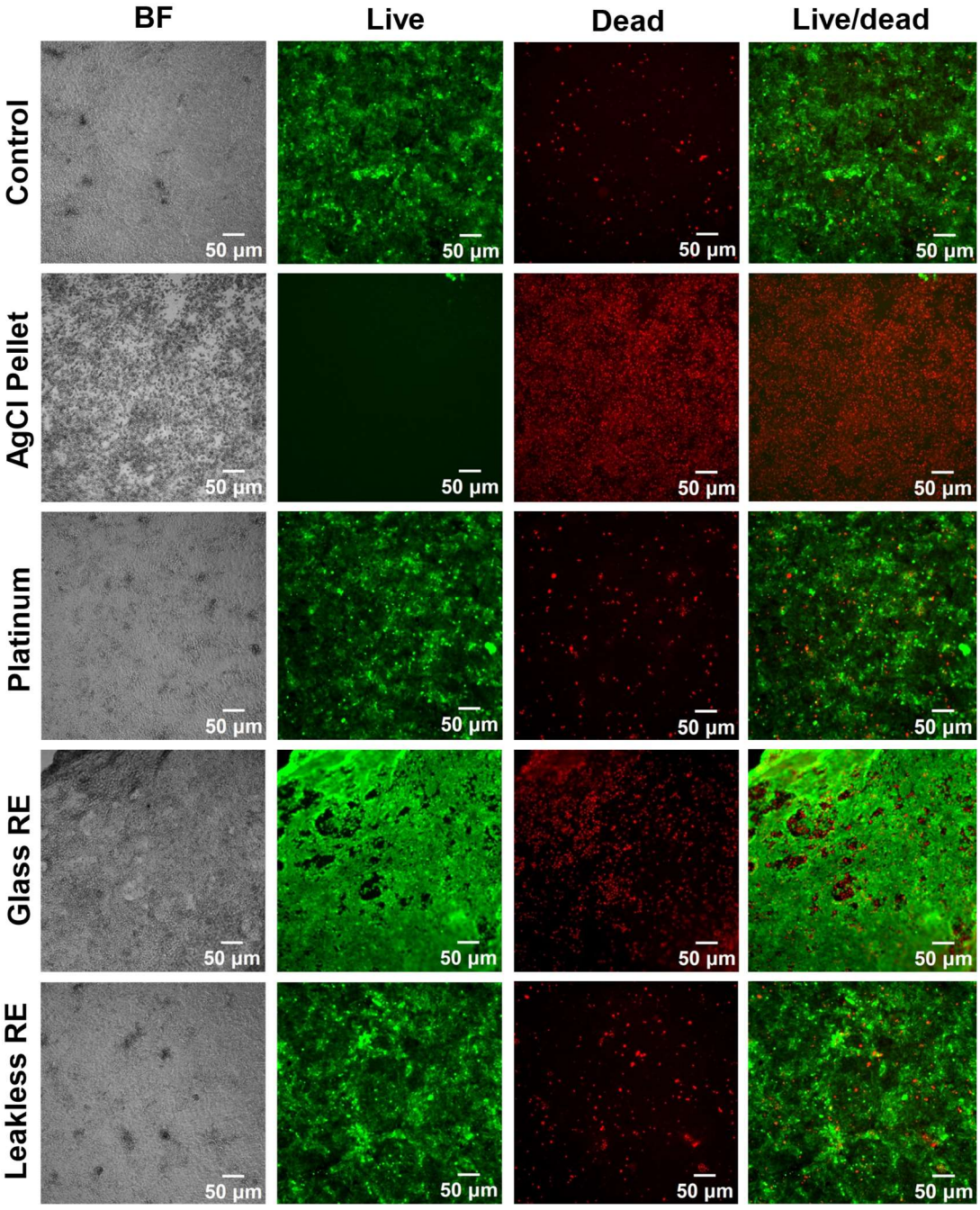

Supplementary Figure 12. Cytotoxicity of various gate electrodes. Viability of epithelial MDCKII cells cultured in the presence of different REs as an indicator of their cytotoxicity. The first column displays bright field (BF) images. The second column displays the images of live cells expressing a green signal, cells expressing a red signal in the third column represent dead cells, and the composites in the fourth column indicate the ratio of LIVE/DEAD cells for each condition.

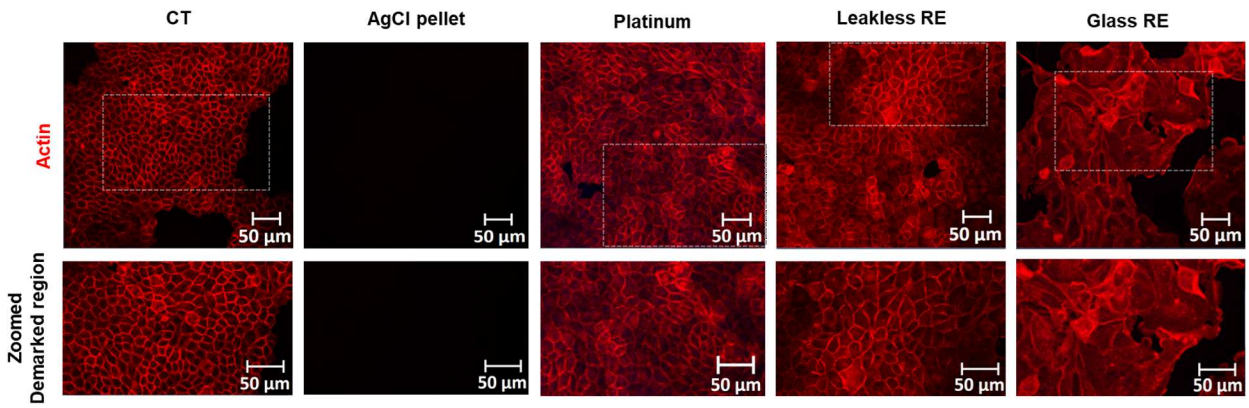

Supplementary Figure 13. Biocompatibility of various gate electrodes. MDCKII morphology and cell coverage as a rough indicator of RE biocompatibility. The top row displays actin-stained cells as a method to delineate their morphology, and the bottom row shows a zoomed image of the demarked area in the top image. Columns display images of actin-stained cells grown in the presence of different REs (CT = control).

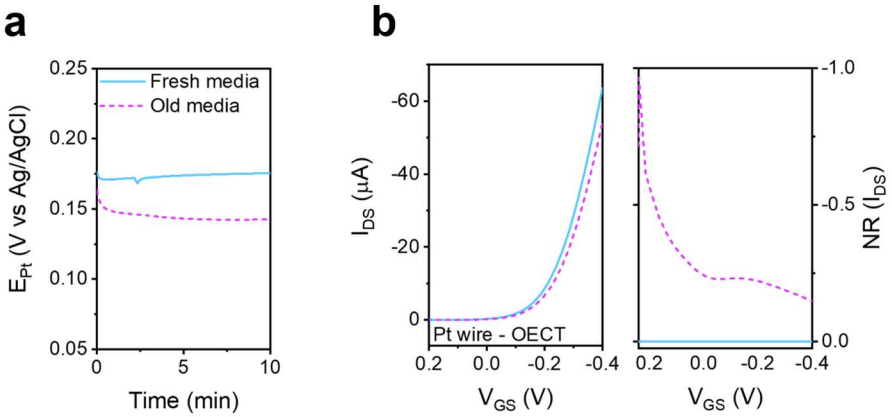

Supplementary Figure 14. Effect of the electrolyte composition change on the OECT response. a) Electrochemical potential of a Pt wire in fresh and old cell media. **b)** Left: p-type OECT response in fresh and old cell media when a Pt wire is used as G. Right: normalized response of the OECT. In this evaluation, we used a fresh cell culture media and a conditioned cell culture media, which is a medium whose chemical composition has changed since it was left in contact with the cell culture for 3 days and contains components secreted by the cells.

In Supplementary Fig. 14a, we report the electrochemical potential of a Pt wire in fresh and conditioned cell media, showing a progressive negative shift as the media ages. The potential of the Pt changes with a shift of 33 mV after 3 days of incubation. The consequence of this shift in the OECT results is reported in Supplementary Fig. 14b-left, where a Pt wire is used to modulate

a p-type enhancement mode OECT when the electrolyte is fresh or old, in the absence of cells. The measurement in the conditioned media has a lower current. If we did these measurements in the presence of the cells, this low current would be mistakenly attributed to a successful formation of the insulating cell layer. However, in reality, it is only related to a reduction of the potential of the G. As reported in Supplementary Fig. 14b-right, this artifact led to a modulation of the I_{DS} up to 100% for the most sensitive V_{GS} values. These conclusions are valid for any other G material, regardless of its safety for the cells (such as PEDOT:PSS, Ag, Ti, Cr, and Au[16]). When the polarizable electrodes are exposed to cell media, their electrochemical potential may vary with the composition of the media itself.

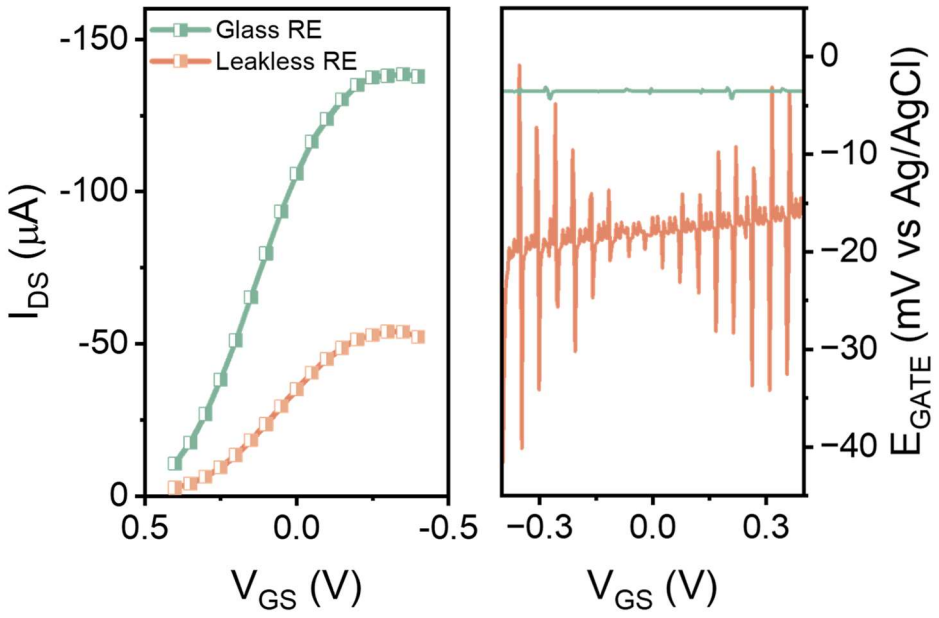

Supplementary Figure 15. OECT response to the use of an high-impedance gate. Left: transfer curve of a PEDOT:PSS OECT when the G is an Ag/AgCl with either a glass porous membrane or a leakless membrane for the ionic connection with the electrolyte. Right: the electrochemical potential of the two G terminals during the transfer curve.

The leakless RE cannot be used as a direct G due to the high resistance of the solid electrolyte membrane (10 kΩ), which causes a high voltage drop on the gate itself, hampering the channel modulation. In Supplementary Fig. 15-left, we report a transfer curve of a PEDOT:PSS-based OECT, when gated with a porous glass membrane RE and with a leakless RE. The leakless RE provides a much smaller modulation of the I_{DS}, and the reason for this is reported in Supplementary Fig. 15-right. While the electrochemical potential of the glass RE remains constant during the

OECT operation, the leakless RE shows a high polarization, up to 41 mV, that affects the transmission of the gate voltage to the OECT channel.

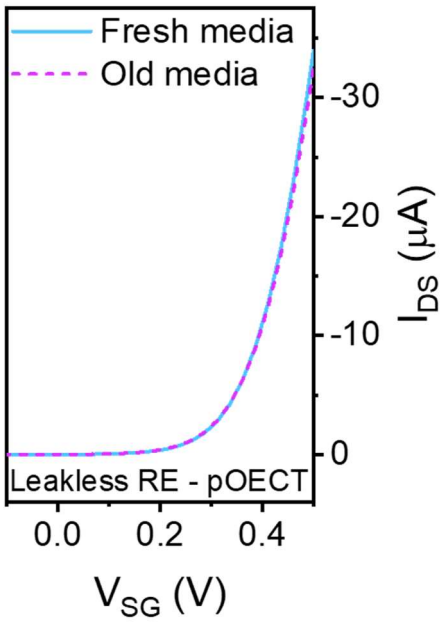

Supplementary Figure 16. Effect of the electrolyte composition change on the pOECT response. p-type pOECT response in fresh or old cell media as electrolyte when the G_S is a leakless Ag/AgCl RE.

In Supplementary Fig. 16, a pOECT is gated by a leakless RE as G_S, a Pt wire is used as G_G and is operated in two different electrolytes, a fresh cell media and the cell media that the cells produced after 3 days of culture. In these conditions, the response of the pOECT is identical, regardless of the freshness of the media, also showing that the OMIEC behavior is not significantly affected by the different composition of the electrolyte. With this setup, if the measurement is taken in the presence of cells on top of the channel, any variation of the pOECT response is solely related to the permeability of the cell layer and completely free from any interference from changes in the gate electrode's properties.

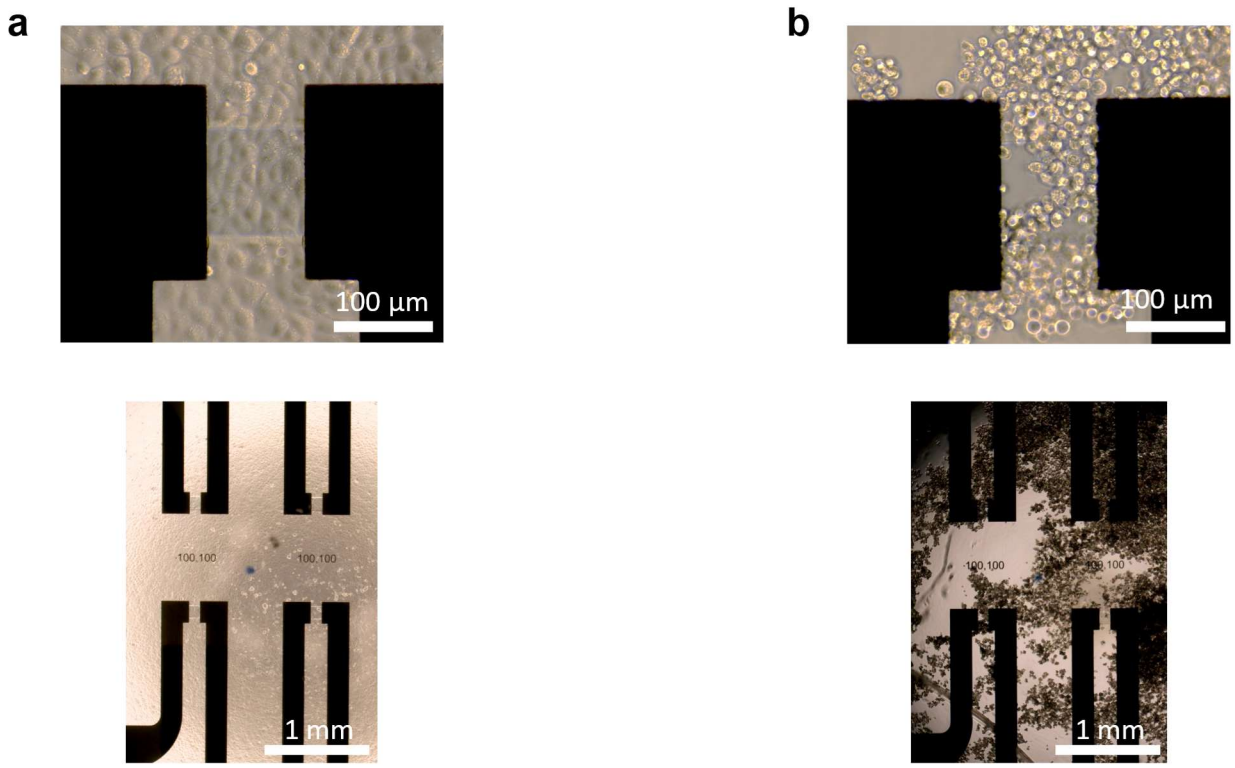

Supplementary Figure 17. Cells coverage of the transistor channels. Phase contrast image of the pOECT channels in the presence of epithelial cells, **a)** before and **b)** after adding trypsin to the cell media.

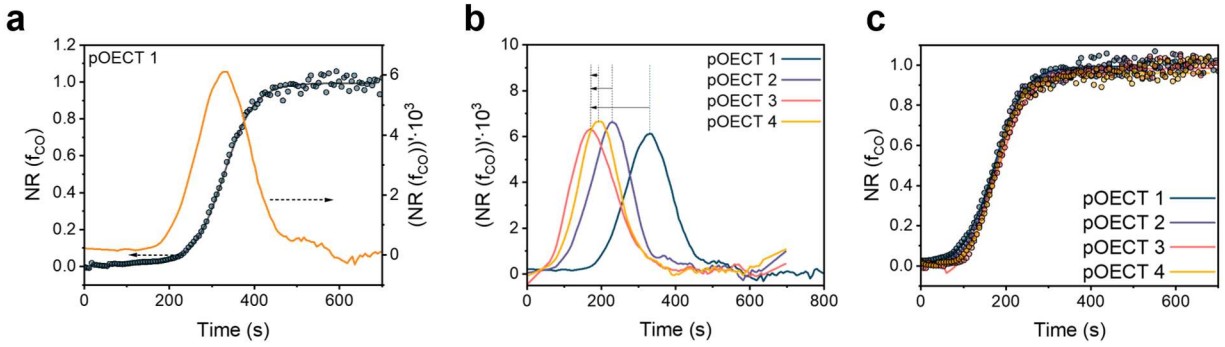

Supplementary Figure 18. Diffusion rates compensation. a) Normalized response of cut-off frequency during time (blue line) and corresponding derivative (orange line). **b)** The peak position of the derivative from each pOECT channel is used to quantify the difference in diffusion time among the four pOECTs. **c)** The pOECT signals are horizontally shifted off the corresponding difference in diffusion time with respect to the pOECT 3, which is chosen as a reference.

References

1. Wu, M. *et al.* Ultrathin, Soft, Bioresorbable Organic Electrochemical Transistors for Transient Spatiotemporal Mapping of Brain Activity. *Advanced Science* **10**, (2023).

2. Khodagholy, D. *et al.* In vivo recordings of brain activity using organic transistors. *Nat Commun* **4**, 1575 (2013).

3. Percival, S. J. & Bard, A. J. Ultra-Sensitive Potentiometric Measurements of Dilute Redox Molecule Solutions and Determination of Sensitivity Factors at Platinum Ultramicroelectrodes. *Anal Chem* **89**, 9843–9849 (2017).

4. Macchia, E. *et al.* Single-molecule detection with a millimetre-sized transistor. *Nat Commun* **9**, 3223 (2018).

5. Macchia, E. *et al.* A handheld intelligent single-molecule binary bioelectronic system for fast and reliable immunometric point-of-care testing. *Sci Adv* **8**, (2022).

6. Genco, E. *et al.* A Single-Molecule Bioelectronic Portable Array for Early Diagnosis of Pancreatic Cancer Precursors. *Advanced Materials* **35**, (2023).

7. Macchia, E. *et al.* Large-Area Interfaces for Single-Molecule Label-free Bioelectronic Detection. *Chem Rev* **122**, 4636–4699 (2022).

8. Mariani, F., Gualandi, I., Tessarolo, M., Fraboni, B. & Scavetta, E. PEDOT: Dye-Based, Flexible Organic Electrochemical Transistor for Highly Sensitive pH Monitoring. *ACS Appl Mater Interfaces* **10**, 22474–22484 (2018).

9. Mariani, F. *et al.* Design of an electrochemically gated organic semiconductor for pH sensing. *Electrochem commun* **116**, 106763 (2020).

10. Mariani, F. *et al.* Advanced Wound Dressing for Real-Time pH Monitoring. *ACS Sens* **6**, 2366–2377 (2021).

11. Gualandi, I. *et al.* Nanoparticle gated semiconducting polymer for a new generation of electrochemical sensors. *Sens Actuators B Chem* **273**, 834–841 (2018).

12. Gualandi, I. *et al.* Organic Electrochemical Transistors as Versatile Analytical Potentiometric Sensors. *Front Bioeng Biotechnol* **7**, (2019).

13. Ng, A. L. *et al.* Chemical Gating of a Synthetic Tube-in-a-Tube Semiconductor. *J Am Chem Soc* **139**, 3045–3051 (2017).

14. Tang, W. *et al.* Solution processed low power organic field-effect transistor bio-chemical sensor of high transconductance efficiency. *npj Flexible Electronics* **6**, 18 (2022).

15. Xu, K. *et al.* Ground-state electron transfer in all-polymer donor–acceptor heterojunctions. *Nat Mater* **19**, 738–744 (2020).

16. Ramuz, M. *et al.* Optimization of a Planar All-Polymer Transistor for Characterization of Barrier Tissue. *ChemPhysChem* **16**, 1210–1216 (2015).